The Journal of Chemical Physics

Ammonium fluoride's analogy to ice: Possibilities and limitations

Cite as: J. Chem. Phys. **154**, 204501 (2021); https://doi.org/10.1063/5.0048516
Submitted: 23 February 2021 . Accepted: 05 May 2021 . Published Online: 25 May 2021

L. J. Conway, K. Brown, J. S. Loveday, and A. Hermann

The Journal of Chemical Physics ARTICLE scitation.org/journal/jcp

Ammonium fluoride's analogy to ice: Possibilities and limitations

Cite as: J. Chem. Phys. 154, 204501 (2021); doi: 10.1063/5.0048516
Submitted: 23 February 2021 • Accepted: 5 May 2021 •
Published Online: 25 May 2021

L. J. Conway, K. Brown, J. S. Loveday, and A. Hermann[a)]

AFFILIATIONS

SUPA, School of Physics and Astronomy and Centre for Science at Extreme Conditions, The University of Edinburgh, Edinburgh EH9 3FD, United Kingdom

Note: This paper is part of the JCP Special Topic on Computational Materials Discovery.
[a)]**Author to whom correspondence should be addressed:** a.hermann@ed.ac.uk

ABSTRACT

Ammonium fluoride, NH_4F, is often seen as an analog to ice, with several of its solid phases closely resembling known ice phases. While its ionic and hydrogen-ordered nature puts topological constraints on the ice-like network structures it can form, it is not clear what consequences these constraints have for NH_4F compound formation and evolution. Here, we explore computationally the reach and eventual limits of the ice analogy for ammonium fluoride. By combining data mining of known and hypothetical ice networks with crystal structure prediction and density functional calculations, we explore the high-pressure phase diagram of NH_4F and host–guest compounds of its hydrides. Pure NH_4F departs from ice-like behavior above 80 GPa with the emergence of close-packed ionic structures. The predicted stability of NH_4F hydrides shows that NH_4F can act as a host to small guest species, albeit in a topologically severely constraint configuration space. Finally, we explore the binary NH_3–HF chemical space, where we find candidate structures for several unsolved polyfluoride phases; among them is the chemical analog to H_2O_2 dihydrate.

I. INTRODUCTION

Water has an extremely rich phase diagram. In its solid phases, every water molecule donates and accepts two hydrogen bonds in a local tetrahedral coordination environment. Globally, no rules other than the Bernal–Fowler ice rules exist, which govern the water molecules' orientations (or hydrogen distributions) to minimize defects, thus resulting in at least 18 known crystalline ice phases[1–3] plus a large number of predicted phases at high[4,5] or negative pressures.[6] In these ice phases, the hydrogen network can be ordered or—typical at elevated temperatures—disordered. Around 60 GPa, the hydrogen bonds begin to symmetrize such that eventually all nearest neighbor O–H–O bonds are linear and symmetric and ice forms an atomic network structure.[7–10] This is not the only possible response to compression: others include auto-ionization (as seen in ammonia, NH_3)[11,12] or decomposition into the elements (as seen in methane, CH_4).[13–15] The flexibility of the hydrogen bond network on display in the structural variety of water is also at the root of many of its anomalous properties and the reason that water can form complex host networks for various small molecular guest species.[16,17] The formation and properties of these gas hydrates have a wide range of implications from industrial gas exploration and carbon sequestration to planetary sciences.[18,19]

Condensed ammonium fluoride, NH_4F, can be thought of as an ice analog as it shares many properties with ice—the local tetrahedral coordination, due to the shape of the NH_4^+ molecular cation, and formation of fully hydrogen-bonded networks. At ambient pressure, its heavy atom lattice is isostructural to the oxygen lattice of ice Ih. It can form solid solutions with ice up to about 20 mol. % concentration and also forms a monohydrate, $NH_4F{\cdot}H_2O$.[20–22] However, NH_4F also differs from ice in important ways. First, it is an ionic structure, $(NH_4^+){\cdot}F^-$. The resulting electrostatics means that the fluorine/nitrogen distribution on the sites of any tetrahedral network is expected to be ordered; any disorder would lead to nearest neighbor F–F or NH_4–NH_4 units with a prohibitively large energy cost from Coulomb repulsion and the presence of Bjerrum-like defects[23] in the resulting hydrogen bond network. Note that any network that has odd-membered rings of hydrogen bonds will inevitably have such defects, as alternate assignments of sites on an odd-membered ring to F and NH_4 are not possible. As a consequence, NH_4F can only

form ice polymorphs that have exclusively even-membered rings of hydrogen bonds. Second, the hydrogen network is ordered, as all hydrogens are covalently bound to nitrogen. NH_4F can therefore not show the same type of thermally induced order/disorder transitions as ice. Third, because of the asymmetry between fluorine and nitrogen, there is no reason why symmetric hydrogen bonds of the type F–H–N should form at high pressure. It is presently unknown how (or if at all) NH_4F loses its molecular character under compression; its phase diagram has not been studied beyond 30 GPa. Finally, while small amounts of NH_4F doping into ice can modify water clathrate cage structures, manipulate hydrogen ordering transitions, and even influence the high-pressure phase diagram,[24–28] it is not known if pure NH_4F or NH_4F-rich solutions can form host–guest compounds similar to gas hydrates.

Here, we present a computational study around the overarching question how far the ice analogy of NH_4F holds, and how it breaks down in various situations. Specifically, we look to probe this analogy in three different directions. First, we explore the high-pressure phase diagram of NH_4F, far beyond the symmetrization pressure of the hydrogen bonds in ice; to this end, we construct hypothetical NH_4F phases based on the ice phase diagram in conjunction with crystal structure searches up to 300 GPa. Second, we investigate the capability of NH_4F to act as a host structure similar to water in gas hydrates; specifically, we study the formation and stability of ammonium fluoride hydrides, NH_4F–H_2. Finally, in recognition of the binary nature of $(NH_3)(HF)$, we explore the full phase diagram of binary compounds $(NH_3)(HF)_n$, using crystal structure prediction methods, which is analogous to surveying the H_2O–H_2O_2 phase diagram in the ice-related chemical space. We show that NH_4F departs qualitatively from ice-like behavior above 80 GPa; that host–guest compounds with relevant inclusion compounds can form, but phase diagrams are driven by topological constraints on host networks; and that ammonium polyfluorides have rich phase diagrams around the formation of the FHF molecule and $(HF)_n$ clusters, and we include the previously unknown analog to the dihydrate of H_2O_2.

II. COMPUTATIONAL METHODOLOGY

We performed density functional theory (DFT) calculations using the CASTEP code.[29] Electronic exchange–correlation effects were described with the Perdew–Burke–Ernzerhof (PBE) functional[30] and ultra-soft pseudopotentials as generated "on-the-fly" by CASTEP. Geometry optimizations were performed with a plane wave cutoff of 1000 eV and Monkhorst–Pack Brillouin zone sampling grids[31] with k-point spacings of no more than $2\pi \times 0.04$ Å^{-1}. In Figs. S1 and S2 in the supplementary material, we present NH_4F phase stabilities from a many-body dispersion (AMD) scheme[32] and using the Becke-Lee-Yang-Parr (BLYP)[33,34] and the Regularized Strongly Constrained and Appropriately Normed (RSCAN)[35] exchange–correlation functionals.

We generate new high-pressure candidate structures for NH_4F by manually building analogs of known ice phases and other ammonium halides and by structure searches based on the particle swarm optimization method using the CALYPSO code.[36] Typical parameters for this candidate structure generation and screening were a plane wave cutoff of 350 eV and k-point spacings of no more than $2\pi \times 0.07$ Å^{-1}.

Optimized water ice structures based on zeolite networks were obtained from the Materials Cloud archive.[37] NH_4F candidates were selected by calculating ring statistics on each of the structures, keeping only structures with exclusively even-membered rings of hydrogen-bonded molecules. Some structures had geometries with poorly defined tetrahedral networks—despite their parent SiO_2 structure tetrahedral network. For example, some structures possessed OH···O bonds with small O–H–O angles or OH groups without a mutual neighbor. We discounted these structures as a further pre-selection criterion. The ice IV structure in the dataset is erroneous, so a correct structure was added manually.

Crystal structure searches were carried out at 30, 100, and 300 GPa generating over 2500 NH_4F structures, each consisting of between 2 and 4 f.u. Generating larger unit cells randomly becomes computationally prohibitive. However, a significant number of ice analogs with larger unit cells were considered via the dataset by Engel *et al.*[37]

For NH_4F–H_2 host–guest compounds at low pressures, where dispersion effects become significant, we use the Tkatchenko–Scheffler (TS) semi-empirical dispersion interaction correction.[38] This method gives transition pressures in the H_2O–H_2 system consistent with similar levels of theory.[39,40]

For the binary $(NH_3)(HF)_n$ system, we perform CALYPSO searches for $n = 1$ to 7 generating over 6500 structures. To determine stable compounds, we compare enthalpy values, $H = U + PV$, where U is the internal energy per molecule and P and V are the pressure and molecular volume, respectively. To compare with a decomposition into the pure molecular phases, we also perform calculations on the known NH_3 and HF crystal structures.

Within the binary systems, the compounds that form the convex hull of the relative formation enthalpies,

$$\Delta H(x) = H(A_xB_{1-x}) - xH(A) - (1-x)H(B), \tag{1}$$

are thermodynamically stable against decomposition. Here, A = (H_2 and HF) and B = NH_4F.

Phonons were calculated for all relevant structures at 2, 10, and 100 GPa. These were performed using CASTEP with norm-conserving pseudopotentials and density functional perturbation theory on q-point grids centered around the Γ point spaced by no more than $2\pi \times 0.1$ Å^{-1}. Gibbs free energies and zero point energies, $G = H - TS_{vib} + E_{ZPE}$, were calculated using the harmonic approximation on the phonon densities of states. These q-point grids were sufficient to give well-converged Gibbs free energies. The stability of compounds in the binary systems is calculated as shown above.

Topological charge density analyses were performed using the QUANTUMESPRESSO package[41] using projector augmented wave (PAW) pseudopotentials. The geometries were re-optimized for these pseudopotentials and the charge densities were calculated with a plane wave cutoff energy of 1500 eV on a dense charge density grid with a cutoff of 18 000 eV. All-electron charge densities were then analyzed with the CRITIC2 code[42] to perform Bader's QTAIM analysis[43] for integrating atomic basins and locating critical points.[44] Electronic localization function (ELF) calculations were also done using QUANTUMESPRESSO and crystal orbital Hamilton populations (COHPs) calculated using the LOBSTER code.[45–48]

III. RESULTS

A. NH_4F under pressure

As many as seven solid phases have been reported for NH_4F,[49] three of which have ice analogs; phase I is a hexagonal structure and ice Ih analog[50] stable up to 0.4 GPa; phase II is a rhombohedral structure[50] stable up to 1 GPa, an analog of the metastable phase IV of ice; phase III is a cubic CsCl-like structure and ice VII analog;[51] phase IV is a plastic phase stable at higher temperatures, in a NaCl-like structure;[52] and phases V-VII are likely stacking disordered structures of phase I.[49,53]

Bellin *et al.* suggested a disorder–order transition above 10 GPa in the cubic NH_4F-III phase.[51] Above the ordering pressure, a small tetragonal distortion has been implied from broadening of Raman peaks[51] and density functional theory was used to give a qualitatively similar phase sequence at low temperatures. The proposed disorder in phase III is qualitatively different from that seen in ice VII. The latter has two interpenetrating hydrogen-bonded sublattices, and the hydrogen network *within* each sublattice is disordered. In NH_4F-III, rotational disorder on the NH_4 sites is proposed to result in disordered hydrogen bonds *between* the sublattices.

To explore the potential phase evolution of NH_4F, we generated candidate structures by building NH_4F analogs from known water ice structures and zeolite frameworks, and by crystal structure searching.

To build potential water analog structures, we surveyed water network geometries in the zeolite-inspired dataset provided by Engel *et al.*[54] This dataset contains 15 869 water ice structures, optimized after substitution of H_2O into SiO_2 zeolite structures. Of the original SiO_2 structures, 3908 contain exclusively even-membered rings along –Si–O–Si– bonds. After H_2O substitutions and subsequent optimizations, 1326 of these even-ringed structures still possess well defined tetrahedral networks at every molecular site. Into these structures, we inserted $NH_4{\cdot}F$ ion pairs, placing them on the oxygen sites such that there is a consistent $NH_4\cdots F$ hydrogen bonding network. These structures were then optimized at 5 GPa. The initial, first two intermediate, and final enthalpies of the geometry optimizations are shown in Fig. 1(a). Many of these NH_4F structures relax via geometry optimization to an equivalent of NH_4F-III, which correctly emerges as the most stable (lowest enthalpy) NH_4F structure at 5 GPa.

The convex hull of enthalpy and volume can be used to estimate the transition pressures to metastable structures, assuming a linear pressure dependence of relative enthalpies.[55] The gradients of lines connecting points on the convex hull give transition pressures relative to the base pressure (5 GPa). The convex hull contains NH_4F-II (from ice IV) and NH_4F-I (from ice Ih) as stable structures. Figure 1(a) shows this and predicts the transitions NH_4F-III → II and NH_4F-II → I at 2.7 and 1.4 GPa, respectively. The rhombohedral structure based on ice II is also found as a candidate structure in addition to three low-density structures: the cubic clathrate structure CS-IV and structures based on the zeolite framework types AST and SOD. These low-density structures are estimated to become stable at negative pressures of −10.8, −1.7, and −1.5 GPa, respectively. In analogy to water clathrate networks at negative pressures, this suggests that these structures could be stabilized at positive pressures if suitable guest molecules occupy their internal cages and voids. The only other remaining valid ice analog structures are ice VI and CS-III. Ice VI is close to the enthalpy–volume convex hull, whereas CS-III is very unstable [see Fig. 1(a)]. Finally, note that no candidate structure for a high-pressure NH_4F phase beyond NH_4F-III emerges from this dataset.

Figure 1(b) shows the relative enthalpies of the structures discussed above as a function of pressure, using the

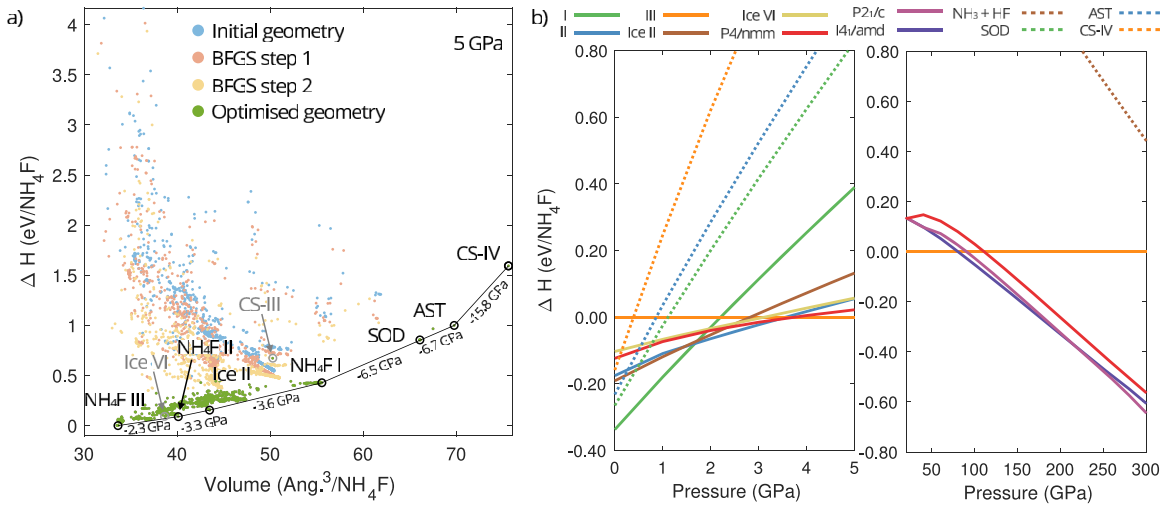

FIG. 1. (a) Enthalpy–volume scatter plot of NH_4F structures at 5 GPa resulting from the H_2O structures from the study by Engel *et al.*[37] Data points relate to enthalpies and volumes for initial geometries (blue), the first two optimization steps (red and yellow), and the optimized geometries (green). Black circles represent the convex hull, with structure types labeled. Gradients of the connections between these structures represent the transition pressures, *relative* to 5 GPa. Gray circles and labels highlight other water ice geometries. (b) Relative enthalpies as a function of pressure in low-pressure (up to 5 GPa) and high-pressure (up to 300 GPa) regimes.

PBE exchange–correlation functional. The phase sequence of NH_4F-I → II → III is reproduced, albeit with overestimated transition pressures compared to experiment, which is similar to what is seen in water ice calculations with the PBE functional.[56] Note that the $P4/nmm$ structure of NH_4Br (a structure with no zeolite or ice analog) emerges as an energetically competitive phase between NH_4F-II and NH_4F-III. This could be an artifact of our calculations or point to a new phase in the low-temperature phase diagram of NH_4F. To examine the robustness of these results, we study the low-pressure phase sequence with several other different functionals and optional dispersion correction schemes. Detailed results are given in Figs. S1 and S2 in the supplementary material and compared to low-temperature experimental data.[51] Among other functionals, the RSCAN functional gives a more accurate NH_4F-I → II transition pressure but underestimates the II → III transition. Conversely, the BLYP functional overestimates all the transition pressures much more than PBE. Semi-empirical dispersion correction schemes generally act to reduce the transition pressures but tend to overestimate the stability of NH_4F-III and the $P4/nmm$ structures. Overall, PBE results are in satisfactory agreement with experiment.

As mentioned above, Fig. 1(a) shows that NH_4F-III represents the highest pressure structure to form from ice analogs and zeolite structure types. To continue the search for higher pressures, we used unbiased crystal structure searches. A total of 2500 structures were generated for NH_4F at 30, 100, and 300 GPa. Searches at 30 GPa successfully reproduced NH_4F-III as the most stable structure, whereas the searches at 100 and 300 GPa reveal two alternative high-pressure structures. First, an $I4_1/amd$ structure stable above 80 GPa (at the PBE level; 89 GPa with BLYP and 86 GPa with RSCAN, see Fig. S3 in the supplementary material), and second, a monoclinic $P2_1/c$ stable above 220 GPa. NH_4F as a compound remains very stable against decomposition into NH_3 + HF up to high pressures [see Fig. 1(b)].

Both new phases, of $I4_1/amd$ and $P2_1/c$ symmetry, are shown in Figs. 2(b) and 2(c). They are dynamically stable in their respective stability regions (see Fig. S7 in the supplementary material), and so are all other new structures presented in this work. Structurally, they are similar with identical heavy atom lattices that are more distorted in the $P2_1/c$ structure. Importantly, they are no longer characterized by the network of $NH_4\cdots F$ hydrogen bonds but rather take up denser structures with the nearest-neighbor shells around either NH_4^+ or F^- ions consisting of both NH_4^+ and F^- ions. The environments surrounding the NH_4/F ions transform from body-centered cubic, with 8 nearest neighbors in NH_4F-III, to quasi-face-centered cubic, with 12 nearest neighbors [see the histograms of separations in Fig. 2(a)]. Due to the global 1:1 stoichiometry of NH_4:F, eight nearest neighbors are of the opposite type, with the remaining four being occupied by the same type as the central ion. Hence, above 80 GPa, the energetic cost of nearest neighbor F–F or NH_4–NH_4 connections, which is so prohibitive at low pressures, is outweighed by the compression work gain due to the closer packing. This is not entirely new: in the autoionized high-pressure $Pma2$ phase of NH_3,[57] which forms an ionic $NH_4{\cdot}NH_2$ solid, each molecular ion has 12 nearest neighbors (quasi-close-packed), of which four are of the same type as the central ion.

However, a general observation is that one of the central rules that govern the topology of $NH_4\cdots F$ structures at low pressures, the alternation of anions and cations, breaks down in these high-pressure structures and so do, therefore, the structural analogies to ice. However, the high-pressure phases still retain hydrogen bonding. In the $I4_1/amd$ structure, all four $NH_4\cdots F$ bonds still form close to linear hydrogen bonds with N–H$\cdots$F angles of 161°, whereas the $P2_1/c$ structure has bonds at 172°, 157°, and 124°. In the latter case, the enthalpy gain from the denser packing of rotated NH_4 cations outweighs the energy cost from non-ideal hydrogen bonds.

A second observation is that, in contrast to ice, pressure does not lead to symmetric hydrogen bonds in NH_4F (note that there is no symmetry argument why this should happen) but instead distorts and weakens them. NH_4F remains a molecular ionic solid up to at

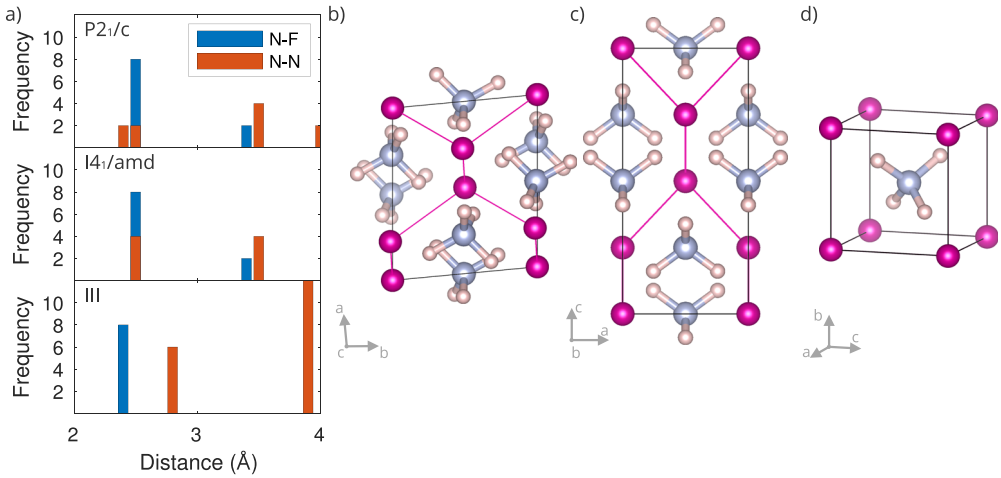

FIG. 2. (a) Pair distribution functions for the heavy atom lattices at 100 GPa. Crystal structures of (b) NH_4F–$P2_1/c$, (c) $I4_1/amd$, and (d) III at 100 GPa. F–F nearest neighbors are connected as a guide to the eye.

least 300 GPa, representing a marked deviation from the structural trends seen in ice. At 100 GPa, the charge transfer from NH_4 to F (based on a Bader analysis) is 0.76*e*, 0.77*e*, and 0.77*e* for NH_4F-III, -$I4_1/amd$, and -$P2_1/c$, respectively. At 300 GPa, the charge transfer in NH_4F-III reduces slightly to 0.74*e*, whereas the charges persist for the high-pressure structures, supporting the ionic picture remaining up to very high pressures. Note that the $I4_1/amd$ structure has the same structure type as LiAg,[58] which has significant ionic character. All of these structures remain wide-gap insulators across the entire pressure range studied here. The partial densities of states and crystal orbital Hamilton populations (COHPs) are shown in Fig. 3. They confirm that the valence states are distinct blocks made up of N-*s*, F-*s*, and N/F-*p* character, while the conduction states are of H-*s* character. The integrated COHP up to the Fermi level gives an indication of the bond strengths, and they are listed in Table S1 in the supplementary material. Typical N–H bond strengths do not change between the different crystal settings. However, there is some variation in the H···F bonding character, which is about 20% stronger in NH_4F-III than the denser structures at 100 GPa, a difference that increases to 40% at 300 GPa. The integrated COHP of N–F contributes less than 3% of the total bond strength. F–F and N–N neighbors contribute effectively nothing. Neither is unexpected as these interactions are of almost pure ionic character, which is not captured by COHP. The 2.1% and 2.2% volume reductions in the $I4_1/amd$ and $P2_1/c$ structures over NH_4F-III (taken at 80 GPa) appear to be enough to compensate for the less favorable electrostatic and bonding configurations than those present in NH_4F-III.

The tendency to form these denser structure types also makes ammonium fluoride stand out among ammonium halides. In both NH_4Br and NH_4Cl, the $P4/nmm$ structure persists in calculations up to high pressures and remains stable against the $I4_1/amd$ and $P2_1/c$ structure types (see Fig. S8 in the supplementary material for relative formation enthalpies). If the ammonium halides simply followed the ionic radii ratio rules, they should all crystalize in the NaCl structure. The tetrahedral charge distribution of the NH_4^+ ion is sufficient to distinguish between the NH_4F, NH_4Br, and NH_4Cl ambient pressure structures and qualitatively predict the

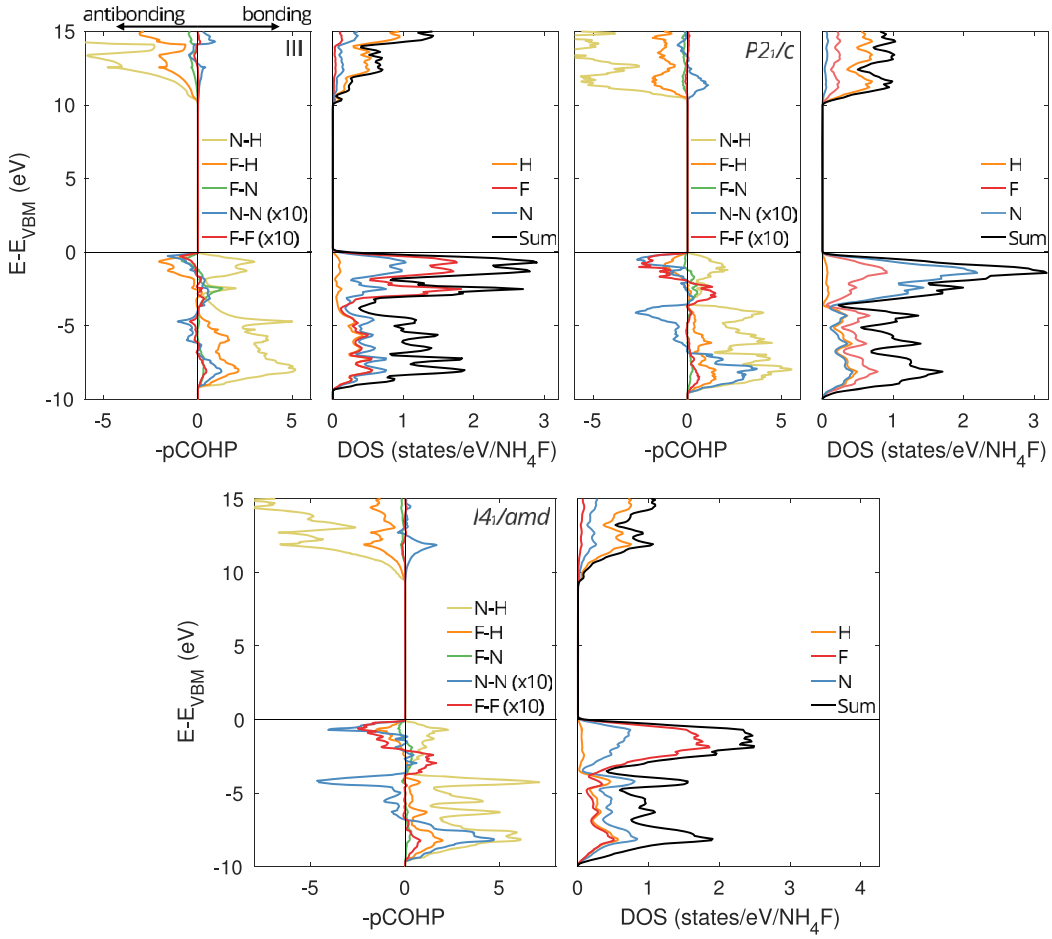

FIG. 3. Crystal orbital Hamilton populations (pCOHP) and partial density of states (pDOS) for the NH_4F structures at 100 GPa. pCOHP values are averaged over all first neighbor shells of each bond type and normalized per NH_4F formula unit. F–F and N–N populations are enhanced by a factor of 10 for clarity.

pressure-induced phase transition to NH_4F-III.[59] Clearly, with pressure, the combined effects of differences in charge distribution, hydrogen bonding, and repulsion strengths continue to differentiate the higher ammonium halides.

B. NH_4F gas inclusions

The analogy of NH_4F with water ice breaks down above 80 GPa, with the advent of its distinct high-pressure phases. At much lower pressures, water can form numerous additional networks in the form of porous hydrogen-bonded cage structures that serve as host networks to encapsulate atomic or molecular guest species such as H_2, Ne, CH_4, or N_2.[16] Among these clathrate hydrates, hydrogen hydrates (H_2O–H_2 mixtures) are of particular technological and fundamental (planetary) interest and have been studied extensively in the past.[16,60–62] The next step in this study is to probe the NH_4F-ice analogy (and its potential breakdowns) via the ability of NH_4F to form host networks around guest species, as typified by potential NH_4F–H_2 mixtures.

At the lowest pressures, hydrogen hydrate forms in the cubic sII clathrate structure, with 136 water molecules and 64 H_2 molecules per unit cell.[61] There are four further known or predicted stable hydrogen hydrates, denoted as C_0, C_1, C_2, and C_3. These compounds have H_2O:H_2 ratios of 2:1, 6:1, 1:1, and 1:2, respectively. C_0 has a chiral water network (S_χ) with channels that the guest molecules can occupy,[3,17,63] whereas the others are based on ice II (C_1)[60] and ice Ic (C_2 and C_3).[39,60] None of these are stable at ambient conditions, but they form under application of a few kbars. There is also a metastable C_{-1} hydrate with an ice I_{sd} water network, a stacking disordered variant of ice I.[64]

DFT calculations with TS dispersion corrections predict a spurious region of stability for an ice Ih-based dihydrate, which is structurally close to but still distinct from C_{-1}. Careful treatment by way of Hartree–Fock and local second-order Møller–Plesset perturbation theory is required to reproduce the experimental observations.[40] Nevertheless, a simple treatment of both systems with PBE and semi-empirical dispersion corrections (SEDCs) gives a reasonable qualitative estimate of the phase stability.

Through the substitution of $2(H_2O) \rightarrow NH_4F$ in the hydrogen hydrates, we constructed candidate NH_4F–H_2 compounds. An NH_4F–C_0 compound is ruled out because the S_χ network possesses odd-membered hydrogen-bonded rings, while C_1 to C_3 are topologically allowed. Of the known stable ultra-low density ice polymorphs, CS-I to -IV, S–H, S–T and S–K,[65] only CS-III and CS-IV are topologically allowed to form NH_4F networks. Despite CS-IV and the zeolite frameworks being predicted as energetically competitive low-density NH_4F structures in Fig. 1(a), not all of these structures have been considered as NH_4F:H_2 networks in this work. Their large cavities will need to be filled with H_2 molecules in unknown amounts and configuration to determine the most stable compounds, which is beyond the scope of this work.

The NH_4F-SOD structure has the smallest cavities, which holds one H_2 molecule per cavity. This structure has the same stoichiometry as C_1 but is still 50 meV/molecule higher in energy (and so does not appear on the scale in Fig. 4). Furthermore, we can speculate on the stability of the CS-IV and AST structures by noting that their networks contain 4-membered rings, and so feature destabilizing F^-–F^- and NH_4^+–NH_4^+ neighbors along the diagonals. Low-density ice structures with four-membered rings are stable only in narrow pressure regions and otherwise mechanically unstable.[66] However, these structures may still play a role as host networks for larger molecules.

On the other hand, filled NH_4F-I (equivalent to ice Ih) is geometrically feasible and dynamically stable. Convex hull constructions for hydrides of both water and NH_4F host structures, obtained from semi-empirical dispersion correction (SEDC) calculations combined with PBE, are shown in Fig. 4. These are qualitatively remarkably similar and confirm that NH_4F can indeed act as a host network to small guest species. However, the phase diagrams also exhibit some differences. At 0 GPa, PBE + SEDC predicts both filled ice Ih and filled NH_4F-I (see Fig. 5) to be stable. With pressure, the filled ice Ih structure gives way to C_0, which is topologically forbidden in the NH_4F–H_2 system. At 2 GPa, both C_1 structures are stable. At 3 GPa, both systems should, in addition, stabilize the C_2 structure. The C_3 analog in NH_4F–H_2 (with the same NH_4F network as C_2) is only metastable between around 20 and 50 GPa. This is a second

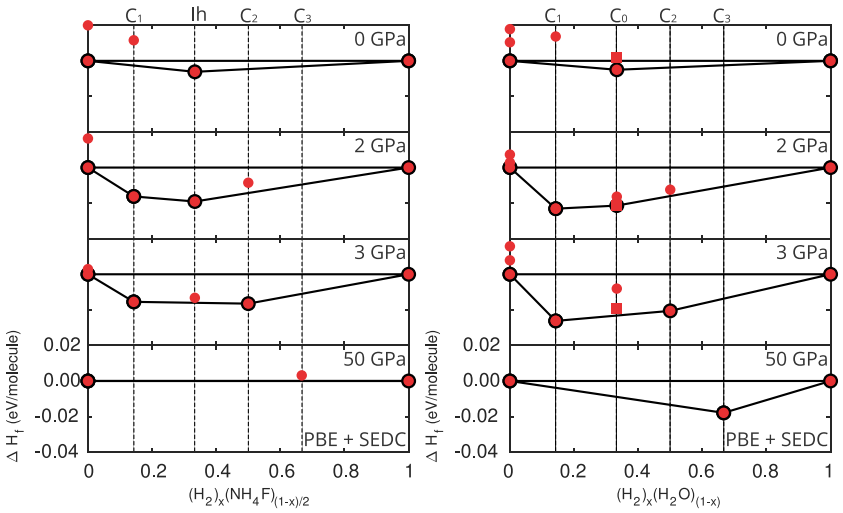

FIG. 4. Relative formation enthalpies for mixtures in the binary systems NH_4F–H_2 (left) and H_2O–H_2 (right) at a series of pressures. Solid black lines and outlined symbols denote convex hulls and calculated stable phases. Square symbols in the H_2O–H_2 panel represent C_0.

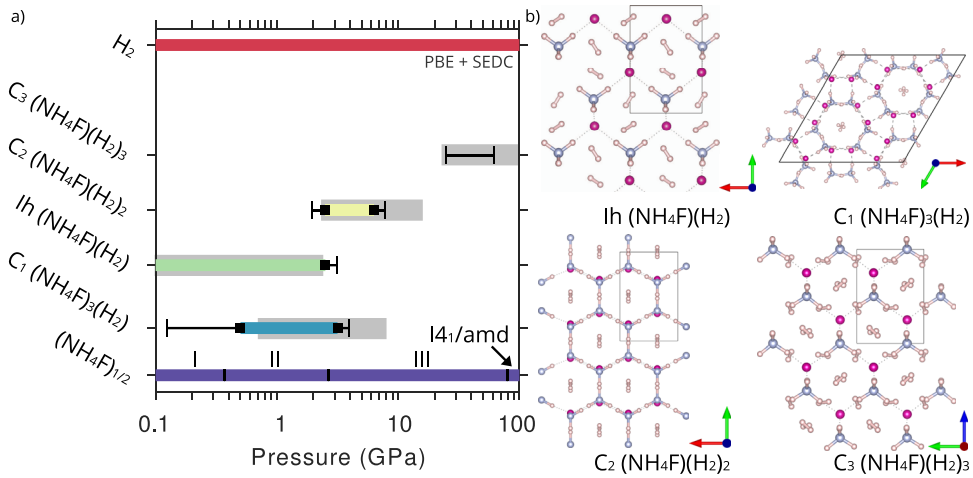

FIG. 5. (a) Ground-state phase diagram for the NH_4F–H_2 binary system as a function of pressure and composition. Colored bars indicate pressure regions of stability. Black lines indicate metastability (see main text). Gray bars represent the corresponding stability regions calculated for the H_2O–H_2 analogs. (b) Unit cells for structures. C_1 is shown in a conventional unit cell setting.

notable difference from the corresponding C_3 hydrogen hydrate, which is stable in calculations from 21 GPa to at least 120 GPa.[39] Free energy estimates that include zero-point vibrational energies and vibrational entropies within the harmonic approximation destabilize the filled Ih structure at 0 K and room temperature at its upper pressure stability limit (see Fig. S5 in the supplementary material) but otherwise do not qualitatively affect the phase stabilities, which agrees with reports for hydrogen hydrates.[39]

Figure 5 summarizes the ground state stability regions of the different NH_4F–H_2 host–guest compounds, obtained from interpolating convex hull data on a fine grid of pressure points, and depicts the various crystal structures. We declare compounds "metastable" if they are less than 10 meV/molecule removed from the convex hull at a given pressure. This captures typical free energy changes between the ground state and room temperature (see Figs. S4–S6 in the supplementary material), which are driven by subtle changes to the low-energy librational phonon modes between different compounds. Filled NH_4F-I is stable in the calculations from 0.1 to 2.7 GPa, "C_1" (the filled ice II equivalent of NH_4F) between 0.9 and 3.7 GPa, and "C_2" (one filled sublattice of NH_4F-III) between 2.5 and 6.7 GPa; all are dynamically stable in those pressure regions (see Fig. S9 in the supplementary material). The latter two are not significantly different from the hydrogen hydrates [shown as gray bars in Fig. 5(a)]. Since these pressure ranges are likely to be overestimated (as seen when compared to hydrogen hydrate experiments), it seems reasonable that NH_4F as a host network can be explored at relatively low pressures, e.g., using neutron diffraction. NH_4F is, therefore, an interesting ice analog for molecular host–guest systems: its filled-ice analog structures are clearly capable of hosting a small molecular species. In fact, this increases its structural variety (the ice II equivalent of NH_4F does not form for NH_4F itself). However, there are again differences to ice, at both ends of the pressure scale: the topological barriers against the formation of the known clathrate cage structures mean that its low-pressure phase diagram will be poorer, unless other, as yet unknown, cage structures with exclusively even-membered hydrogen-bonded rings can form. In this regard, it would be very interesting to study, e.g., the NH_4F–CH_4 system: a larger guest species would require the formation of larger voids or cages in a potential NH_4F host network. At the high-pressure end, the stability of NH_4F hydrides also seems limited, with a "C_3" phase never becoming stable.

Hydrogen inclusions in NH_4F are effectively inserted into an ionic solid. A recent study related the ability of non-polar species (in that case, noble gas atoms) to penetrate ionic lattices to the lowering of the Madelung energy by reducing electrostatic repulsion[67]—however, this was identified as a driving force specifically for ionic compounds with uneven cation and anion numbers (formula AB_2, etc.). Here, this argument does not hold; instead, the tetrahedrally coordinated NH_4F phases simply have large enough cavities to host small guest species. There is no evidence for significant host–guest interactions, with the integrated COHP between neighboring N and H_2 sites having values of less than 0.02 eV.

C. Expanding chemical space: NH_3–HF binary compounds

Ammonium fluoride is the end member of a large family of ammonia-fluoride compounds. The NH_4F–HF binary system and structures comprising this system have been studied experimentally by at least three generations of scientists, mostly using differential thermal analysis (DTA)[68–72] and suggesting stable or metastable compounds for $n = 1$–5 and $n = 7$. Continuing with the ice analogy theme, this corresponds to traversing the chemical space H_2O_{1+x} from $x = 0$ (water, at $n = 0$) to $x = 1$ (hydrogen peroxide, at $n \to \infty$). Arguably, the analogy becomes more stoichiometric rather than chemically significant. In the H_2O–H_2O_2 binary system, a stable structure of hydrogen peroxide dihydrate has been observed[73–75] and

attracted renewed interest since the discovery of H_2O_2 on Jupiter's icy moon Europa.[76–78] Within the present $NH_4F(HF)_n$ analogy, the H_2O_2 dihydrate corresponds to $n = 2$. So far, there has been no comprehensive computational study on the $NH_4F{\cdot}(HF)_n$ structures, and there have been even fewer studies involving pressure, which may provide new synthesis pathways for these compounds.

This is of interest as polyhalides have a wide range of applications. In particular, polyfluorides are used in drug design and to form fluorocarbons such as PTFE.[79] Metal fluorides are good candidates for next generation high energy density battery cells[80] where ammonium fluoride has been used in the synthesis process.[81] A related class of compounds are hydrogen halide halogenates of the form $[X(HX)_n]^-$. The salts found in the NH_4F–HF system will give rise to several hydrogen fluorides consisting of a large positive charge on the hydrogen and negative charge on the fluorine atoms. A well-known example of this is the $[HF_2]^-$ molecule, wherein the central hydrogen is bonded symmetrically to both fluorines with mixed covalent and hydrogen bond character.[82] The higher fluorides form anion clusters consisting of a central fluorine with strong hydrogen bonds to surrounding hydrogen fluoride molecules.

Experimentally, the melting diagram of the $NH_4F(HF)_n$ binary[68] was studied by Ruff and Otto in 1933. They found HF-rich compounds to be stable up to around 290 K for $n = 1, 2, 3$, and 5. In 1961, Euler and Westrum repeated the study, only to find stable phases at $n = 1, 3$, and 5.[69] In 1984, Mootz and Poll found $n = 3, 4$, and 7,[70] supported by XRD measurements that provided crystal structures for these solid phases. There is some discrepancy between these three generations of experiments, which are summarized in Fig. 6(a). Only two phases are found consistently, $n = 1$ and $n = 3$, whereas the others are particular to each experiment. This sensitivity could indicate that the observed compounds at $n = 2, 4, 5$, and 7 may be, in fact, metastable at these conditions or that impurities in the sample stabilize (or destabilize) selected compounds.

An *ab initio* calculation on isolated $(H_nF_{n+1})^-$ polyfluoride clusters with $n = 1$–4 suggests that the stable configurations of isolated anions are linear, angular, planar trigonal, and tetrahedral, respectively,[83] all forming globular hydrogen-bonded clusters centered around an F^- anion. The H-bond dissociation energy decreases with the increasing cluster size such that an $n = 6$ anion would reportedly be unstable against decomposition into $(H_4F_5)^-{\cdot}HF$. Another *ab initio* study considers some specific configurations of the $n = 6$ and 7 clusters.[84] Among the known $NH_4F(HF)_n$ structures,[70] all stable fluoride clusters appear, except for the angular $(H_2F_3)^-$ anion (for $n = 2$) that is missing. The $n = 2$ polyfluoride corresponds to the only known stoichiometric composition in the analogous H_2O–H_2O_2 system. Under pressure, however, new compositions may become stable, paving new routes to fluorine chemistry.

Here, we explored the full NH_3–HF chemical space with unbiased structure searching at 30 and 50 GPa at 1:6, 1:5, 1:4, 1:3, 1:2, 1:1, 2:1, and 3:1 compositions, generating over 6000 candidate structures. We note that apart from a previously known ammonia rich structure, $(N_2H_7)(F)$,[85] which we calculate to be stable up to 4 GPa, no other NH_3-rich structures appear on or close to the convex hull. Therefore, we focus on the fluoride-rich NH_4F–HF phase diagram. Convex hulls at specific pressures are shown in Fig. 6(b) and the phase stability chart in Fig. 6(c). Vibrational entropy effects, shown for a representative pressure in Fig. S6 in the supplementary material, do not qualitatively change the convex hull.

Relative formation enthalpies of the polyfluorides $n = 1$–3 are shown in Fig. 7. In ammonium bifluoride $(NH_4)(HF_2)$ ($n = 1$), a pressure-induced phase transition was reported, from the known orthorhombic phase I (space group *Pman*) to an unknown structure—labeled phase III—around 5–10 GPa.[72] We reproduce the stability of phase I at low pressures. The central structural motif for phase I is of tetrahedral ammonium cations hydrogen-bonded to four $(HF_2)^-$ anions (see Fig. 8). Connecting neighboring fluoride ions reveals a layered two-dimensional motif consisting of

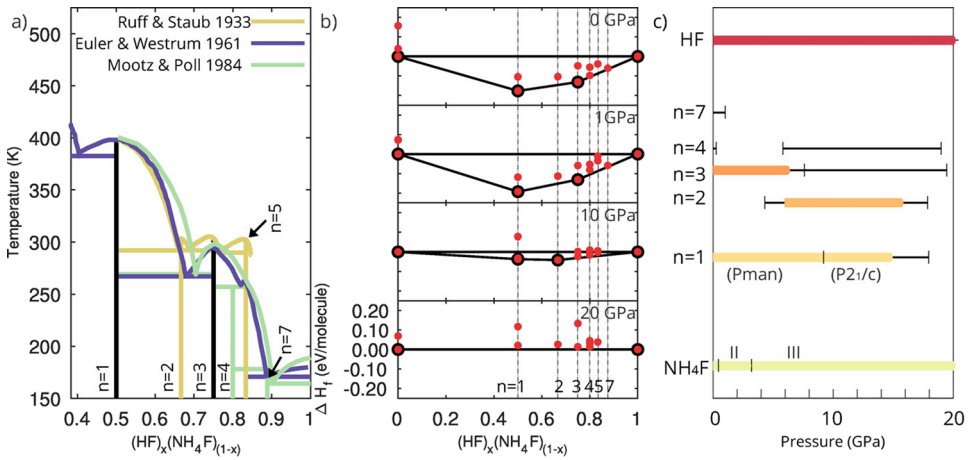

FIG. 6. Ground state energetics of the NH_4F–HF system. (a) Experimental composition phase diagrams adapted from Refs. 68–70. Black lines mark phases seen in all experiments to the highest measured melt temperature. Solid compositions $NH_4F(HF)_n$ include $n = 1$–5 and 7. (b) Calculated convex hulls of relative formation enthalpies of NH_4F–HF compounds. The structures are of the form $(NH_4)^+(H_nF_{n+1})^-$, where n is given along vertical dashed lines. (c) Calculated ground state phase diagram as a function of pressure. Stable phases are colored lines and metastable phases (less than 10 meV removed from the convex hull) are thin black lines.

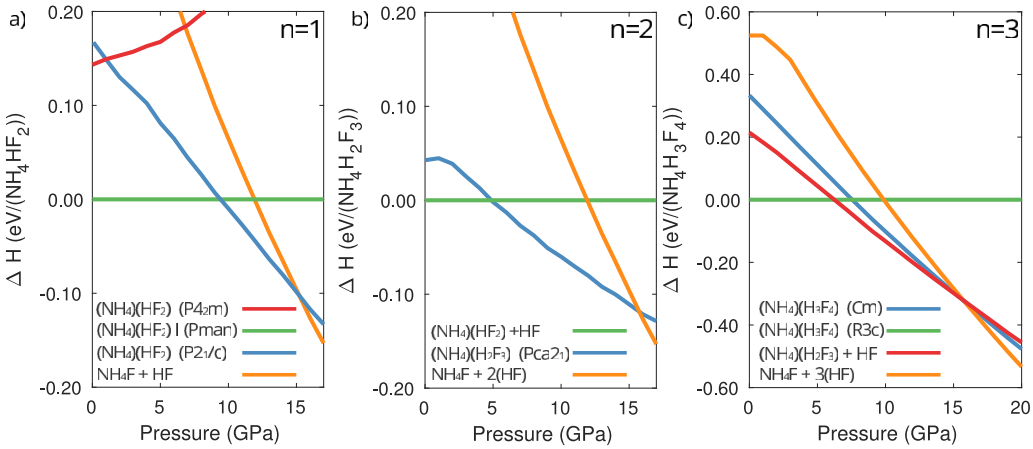

FIG. 7. Relative enthalpies as a function of pressure for the $NH_4F(H_nF_{n+1})$ compounds (a) $(NH_4F)^+(HF_2)^-$, (b) $(NH_4F)(H_2F_3)$, and (c) $(NH_4F)(H_3F_4)$.

tessellating squares and triangles, where the squares are formed of F–F neighbors and the triangles are formed of F–F neighbors and bridging hydrogens in the F–H–F bonds. At 10 GPa, we predict a transition from phase I to a monoclinic structure with $P2_1/c$ symmetry, which we propose as the structure of phase III. This structure is best understood as a sheared distortion of a tetragonal parent structure $P\bar{4}2m$ that is metastable at low pressures [see Fig. 7(a) and also Fig. 8]. The phase III structure consists of layers of $(NH_4)^+$ and $(HF_2)^-$ ions, the latter aligned along the c axis. Under pressure, this structure becomes unstable toward a shear strain between layers, and in the optimized structure, the $(HF_2)^-$ ions are tilted (see Fig. 8). The $P2_1/c$ structure is dynamically stable; phonon dispersions are shown in Fig. S10 in the supplementary material. This new phase III is not expected to survive much further under continued compression: beyond 15 GPa, a 1:1 mixture of NH_4F-III and HF is most stable. All relevant $(NH_4)(HF_2)$ structures retain the

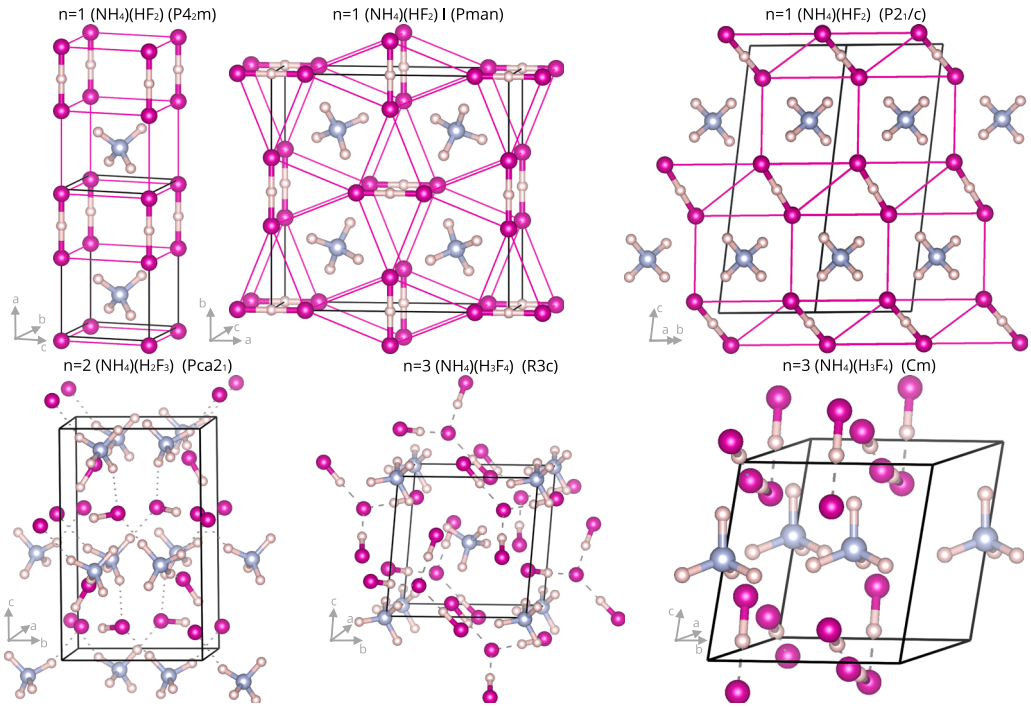

FIG. 8. Crystal structures for HF-rich mixtures $NH_4F(HF)_n$, labeled by n and space group. Some structural motifs highlighted by thin pink lines show the connection between neighboring fluorine atoms.

structural motifs of phase I, in particular, the linear $(HF_2)^-$ anion (in line with most of the biflourides except Rb·HF_2),[71] but differ in the packing arrangements.

The $(NH_4)(H_2F_3)$ ($n = 2$) compound has only been seen in historical DTA experiments[68] but may be at least metastable at ambient conditions. Our structure searches reveal that the compound can be stabilized above 6 GPa in a $Pca2_1$ structure before decomposing at 15.5 GPa to $(NH_4)F + 2(HF)$ [see Fig. 7(b)]. This structure forms an ionic crystal made from hydrogen-bonded chains of $NH_4\cdots F–H\cdots F\cdots H–F\cdots H_4N$. The central anion, F_3H_2, is similar to that seen in $Na^+(H_2F_3)^-$[86] although the overall structure is different. The structure is dynamically stable (see the phonon dispersions in Fig. S10 in the supplementary material) and, like the bifluoride phase III predicted above for $n = 1$, is a wide-gap insulator (see the electronic densities of states in Fig. S11 in the supplementary material).

For $(NH_4)(H_3F_4)$ ($n = 3$), the experimental $R3c$ structure is confirmed in our calculations to be stable from 0 GPa up to around 6 GPa [see Fig. 7(c)]. Our structure searches reveal a monoclinic structure (space group Cm) that supersedes the $R3c$ structure at 7.5 GPa. In contrast to the other known hydrogen fluoride salts, this structure has both an HF_2 anion and an HF molecule. Increased pressure likely reduces the space available to form the globular arrangements seen in the other structures. However, the Cm phase turns out to be metastable against the newly predicted $n = 2$ compound discussed in the previous paragraph above 6 GPa, which suggests that the missing $n = 2$ compound could be synthesized along a secondary route, either by starting from the $n = 1$ compound in the presence of extra HF or directly from compressing the $n = 3$ compound.

Overall, for the higher fluorides ($n = 3, 4, 7$), the NH_4F–HF binary phase diagram shown in Fig. 6 agrees with experimental findings, as all of the known $(NH_4)(H_3F_4)$, $(NH_4)(H_4F_5)$, and $(NH_4)(H_7F_8)$ structures are at least metastable at ambient pressure conditions. Figure S6 in the supplementary material shows relative Gibbs free energies for the NH_4F–HF binary at 10 GPa. Finite temperature effects do not impact stability significantly; ZPE stabilize the $(NH_4)(H_3F_4)$-Cm structure against decomposition at T = 0 K, but not at room temperature. The supplementary material further contains more detailed analyses of the chemical bonding in these phases, in particular, within the anionic H_nF_{n+1} clusters. Under pressure, these higher fluorides are destabilized, likely due to the presence of the large anionic clusters. Instead, the missing stoichiometry $n = 2$, $(NH_4)(H_2F_3)$, becomes stable. This compound is the analog to $(H_2O)_2$·(H_2O_2), the only known stoichiometric hydrogen peroxide hydrate. The fact that this compound is so much less stable than several other polyfluorides, and stable only at high pressure, illustrates again how much weaker the analogy of ammonia fluorides and ice has become in this expanded chemical space.

IV. CONCLUSION

In summary, we have explored here how far the analogy of ammonium fluoride, NH_4F, to water ice, H_2O, holds. To this end, we have studied the high-pressure phase diagram of NH_4F, examined its suitability to act as a host network to small molecular guest species, and expanded into the full NH_3–HF chemical space. Crystal structure prediction with density functional theory calculations was supplemented by detailed analyses of electronic structures and chemical bonding.

While at typical pressures studied experimentally, NH_4F shares features of water ice, there are a few differences as pressure increases. First, the topological restrictions on allowed NH_4F structures limit the number of potential ice analogs. Second, H_2O ice eventually, between 60 and 100 GPa, forms symmetrized hydrogen bonds in the ice VIII → ice X transition. Such a symmetrization is not possible for NH_4F. Both limitations have consequences for the NH_4F phase diagram, deviating from water's phase diagram at high pressures. Indeed, we find that the ice VII analog NH_4F-III gives way, around 80 GPa, to close-packed structures that break the network topology restrictions against like ion nearest neighbors and where $N–H\cdots F$ hydrogen bonding is less significant. Nonetheless, we find that NH_4F remains a molecular solid and stable against decomposition up to at least 300 GPa.

We furthermore show that NH_4F can form stable host–guest hydride compounds of the form $(NH_4F)_m(H_2)_n$, where the NH_4F host networks are analogous to those of hydrogen hydrates. Similar constraints as discussed above affect the NH_4F–H_2 system, which is topologically forbidden to form the S_χ, CS-I, or CS-II host networks. While an NH_4F doped H_2O CS-I cage has been studied,[25] it remains to be seen if NH_4F rich compounds could form with H_2O doping and how dramatically the phase diagram will change as a result. The hydrogen bond symmetrization predicted in hydrogen hydrate C_3 at high pressures is also not feasible. The ammonium fluoride hydride $(NH_4F)(H_2)_2$ in the C_3 analog structure does not appear to be stable at any pressure, possibly for this reason. However, structural analogs of ice I_h, C_1, and C_2 hydrogen hydrates emerge as stable and in the same pressure sequence and on roughly the same pressure scale as in the hydrogen hydrates.

Finally, we explore the NH_3–HF binary system, which (chemically) corresponds to the H_2O–H_2O_2 binary system. While the former is very rich, the latter features a single stoichiometric mixture, 1:2. Its equivalent here, ammonium bifluoride, had not been identified unambiguously in experiments. We show here that ammonium bifluoride becomes stable at pressures accessible to high-pressure syntheses. In addition, we present a structural candidate for the previously unresolved high-pressure phase of $(NH_4)(HF_2)$. With the increasing HF content, these polyfluorides show an intriguing evolution of anionic H_nF_{n+1} cluster structures dominated by hydrogen bonding.

The relation and analogies between NH_4F and water ice remain complex. On one hand, we have shown here that NH_4F can form filled ice-like host–guest structures very similar to the hydrate equivalents. On the other hand, at high pressures, NH_4F departs remarkably from the structural trends seen in ice. Finally, there are chemical avenues available to NH_4F, such as continuous addition of HF, which are very interesting in their own right, without immediately obvious connections to the physics or chemistry of water.

SUPPLEMENTARY MATERIAL

See the supplementary material for results from other exchange–correlation functionals and dispersion correction schemes, Gibbs free energy analyses, phonon dispersions for all new

structures, tabulated COHP data, partial electronic DOS and ELF data, further electronic structure and bonding analyses, and crystal structure information for all new structures.

ACKNOWLEDGMENTS

L.J.C. and K.B. were supported by the UK's EPSRC through the Condensed Matter Centre for Doctoral Training (Grant No. EP/L015110/1). Computational resources provided by the UK's National Supercomputer Service through the UK Car-Parrinello consortium (Grant No. EP/P022561/1) and Project No. d56 "Planetary Interiors" and by the UK Materials and Molecular Modeling Hub (Grant No. EP/P020194) are gratefully acknowledged.

DATA AVAILABILITY

The data that support the findings of this study are openly available in the Edinburgh DataShare at https://doi.org/10.7488/ds/3033.

REFERENCES

[1] J. D. Bernal and R. H. Fowler, J. Chem. Phys. **1**, 515 (1933).
[2] V. F. Petrenko and R. W. Whitworth, *Physics of Ice* (Oxford University Press, 1999).
[3] L. Del Rosso, M. Celli, and L. Ulivi, Nat. Commun. **7**, 13394 (2016).
[4] M. Benoit, M. Bernasconi, P. Focher, and M. Parrinello, Phys. Rev. Lett. **76**, 2934 (1996).
[5] A. Hermann, N. W. Ashcroft, and R. Hoffmann, Proc. Natl. Acad. Sci. U. S. A. **109**, 745 (2012).
[6] T. Matsui, M. Hirata, T. Yagasaki, M. Matsumoto, and H. Tanaka, J. Chem. Phys. **147**, 091101 (2017).
[7] K. Aoki, H. Yamawaki, M. Sakashita, and H. Fujihisa, Phys. Rev. B **54**, 15673 (1996).
[8] A. F. Goncharov, V. V. Struzhkin, M. S. Somayazulu, R. J. Hemley, and H. K. Mao, Science **273**, 218 (1996).
[9] V. V. Struzhkin, A. F. Goncharov, R. J. Hemley, and H.-k. Mao, Phys. Rev. Lett. **78**, 4446 (1997).
[10] P. Loubeyre, R. LeToullec, E. Wolanin, M. Hanfland, and D. Hausermann, Nature **397**, 503 (1999).
[11] S. Ninet, F. Datchi, P. Dumas, M. Mezouar, G. Garbarino, A. Mafety, C. J. Pickard, R. J. Needs, and A. M. Saitta, Phys. Rev. B **89**, 174103 (2014).
[12] T. Palasyuk, I. Troyan, M. Eremets, V. Drozd, S. Medvedev, P. Zaleski–Ejgierd, E. Magos–Palasyuk, H. Wang, S. A. Bonev, D. Dudenko, and P. Naumov, Nat. Commun. **5**, 3460 (2014).
[13] F. Ancilotto, Science **275**, 1288 (1997).
[14] H. Hirai, K. Konagai, T. Kawamura, Y. Yamamoto, and T. Yagi, Phys. Earth Planet. Inter. **174**, 242 (2009).
[15] L. J. Conway and A. Hermann, Geosciences **9**, 227 (2019).
[16] J. S. Loveday and R. J. Nelmes, Phys. Chem. Chem. Phys. **10**, 937 (2008).
[17] D. M. Amos, M.-E. Donnelly, P. Teeratchanan, C. L. Bull, A. Falenty, W. F. Kuhs, A. Hermann, and J. S. Loveday, J. Phys. Chem. Lett. **8**, 4295 (2017).
[18] S. Sun, Y. Hao, and J. Zhao, J. Chem. Eng. Data **63**, 684 (2018).
[19] J. S. Loveday, R. J. Nelmes, M. Guthrie, S. A. Belmonte, D. R. Allan, D. D. Klug, J. S. Tse, and Y. P. Handa, Nature **410**, 661 (2001).
[20] R. Brill and S. Zaromb, Nature **173**, 316 (1954).
[21] S. Zaromb and R. Brill, J. Chem. Phys. **24**, 895 (1956).
[22] L. C. Labowitz and E. F. Westrum, J. Phys. Chem. **65**, 408 (1961).
[23] N. Bjerrum, Science **115**, 385 (1952).
[24] K. Shin, I. L. Moudrakovski, M. D. Davari, S. Alavi, C. I. Ratcliffe, and J. A. Ripmeester, CrystEngComm **16**, 7209 (2014).
[25] S. Park, D. Lim, Y. Seo, and H. Lee, Chem. Commun. **51**, 8761 (2015).
[26] J. J. Shephard, B. Slater, P. Harvey, M. Hart, C. L. Bull, S. T. Bramwell, and C. G. Salzmann, Nat. Phys. **14**, 569 (2018).
[27] C. G. Salzmann, Z. Sharif, C. L. Bull, S. T. Bramwell, A. Rosu-Finsen, and N. P. Funnell, J. Phys. Chem. C **123**, 16486 (2019).
[28] Z. Sharif, J. J. Shephard, B. Slater, C. L. Bull, M. Hart, and C. G. Salzmann, J. Chem. Phys. **154**, 114502 (2021).
[29] S. J. Clark, M. D. Segall, C. J. Pickard, P. J. Hasnip, M. I. J. Probert, K. Refson, and M. C. Payne, Z. Krist. - Cryst. Mater. **220**, 567 (2005).
[30] J. P. Perdew, K. Burke, and M. Ernzerhof, Phys. Rev. Lett. **77**, 3865 (1996).
[31] H. J. Monkhorst and J. D. Pack, Phys. Rev. B **13**, 5188 (1976).
[32] A. Tkatchenko, R. A. DiStasio, R. Car, and M. Scheffler, Phys. Rev. Lett. **108**, 236402 (2012).
[33] A. D. Becke, Phys. Rev. A **38**, 3098 (1988).
[34] C. Lee, W. Yang, and R. G. Parr, Phys. Rev. B **37**, 785 (1988).
[35] A. P. Bartók and J. R. Yates, J. Chem. Phys. **150**, 161101 (2019); arXiv:1903.01007.
[36] Y. Wang, J. Lv, L. Zhu, and Y. Ma, Phys. Rev. B **82**, 094116 (2010).
[37] E. A. Engel, A. Anelli, M. Ceriotti, C. J. Pickard, and R. J. Needs, Mater. Cloud Arch. **2018.0010/v1** (2018).
[38] A. Tkatchenko and M. Scheffler, Phys. Rev. Lett. **102**, 073005 (2009).
[39] G. R. Qian, A. O. Lyakhov, Q. Zhu, A. R. Oganov, and X. Dong, Sci. Rep. **4**, 5606 (2014).
[40] J. Košata, P. Merkl, P. Teeratchanan, and A. Hermann, J. Phys. Chem. Lett. **9**, 5624 (2018).
[41] P. Giannozzi, S. Baroni, N. Bonini, M. Calandra, R. Car, C. Cavazzoni, D. Ceresoli, G. L. Chiarotti, M. Cococcioni, I. Dabo, A. Dal Corso, S. de Gironcoli, S. Fabris, G. Fratesi, R. Gebauer, U. Gerstmann, C. Gougoussis, A. Kokalj, M. Lazzeri, L. Martin-Samos, N. Marzari, F. Mauri, R. Mazzarello, S. Paolini, A. Pasquarello, L. Paulatto, C. Sbraccia, S. Scandolo, G. Sclauzero, A. P. Seitsonen, A. Smogunov, P. Umari, and R. M. Wentzcovitch, J. Phys.: Condens. Matter **21**, 395502 (2009).
[42] A. Otero-De-La-Roza, E. R. Johnson, and V. Luaña, Comput. Phys. Commun. **185**, 1007 (2014).
[43] R. F. Bader, *Atoms in Molecules: A Quantum Theory* (Oxford University Press, 1994).
[44] W. Tang, E. Sanville, and G. Henkelman, J. Phys.: Condens. Matter **21**, 084204 (2009).
[45] R. Dronskowski and P. E. Bloechl, J. Phys. Chem. **97**, 8617 (1993).
[46] V. L. Deringer, A. L. Tchougréeff, and R. Dronskowski, J. Phys. Chem. A **115**, 5461 (2011).
[47] S. Maintz, V. L. Deringer, A. L. Tchougréeff, and R. Dronskowski, J. Comput. Chem. **34**, 2557 (2013).
[48] S. Maintz, V. L. Deringer, A. L. Tchougréeff, and R. Dronskowski, J. Comput. Chem. **37**, 1030 (2016).
[49] M. A. Nabar, L. D. Calvert, and E. Whalley, J. Chem. Phys. **51**, 1353 (1969).
[50] A. C. Lawson, R. B. Roof, J. D. Jorgensen, B. Morosin, and J. E. Schirber, Acta Crystallogr., Sect. B: Struct. Sci. **45**, 212 (1989).
[51] C. Bellin, A. Mafety, C. Narayana, P. Giura, G. Rousse, J.-P. Itié, A. Polian, A. M. Saitta, and A. Shukla, Phys. Rev. B **96**, 094110 (2017).
[52] L. D. Calvert and E. Whalley, J. Chem. Phys. **53**, 2151 (1970).
[53] J. J. Shephard, S. Ling, G. C. Sosso, A. Michaelides, B. Slater, and C. G. Salzmann, J. Phys. Chem. Lett. **8**, 1645 (2017); arXiv:1701.05398.
[54] E. A. Engel, A. Anelli, M. Ceriotti, C. J. Pickard, and R. J. Needs, Nat. Commun. **9**, 2173 (2018).
[55] C. J. Pickard and R. J. Needs, J. Phys.: Condens. Matter **23**, 053201 (2011); arXiv:1101.3987.
[56] B. Santra, J. Klimeš, D. Alfè, A. Tkatchenko, B. Slater, A. Michaelides, R. Car, and M. Scheffler, Phys. Rev. Lett. **107**, 185701 (2011).
[57] C. J. Pickard and R. J. Needs, Nat. Mater. **7**, 775 (2008).
[58] V. V. Pavlyuk, G. S. Dmytriv, I. I. Tarasiuk, I. V. Chumak, H. Pauly, and H. Ehrenberg, Solid State Sci. **12**, 274 (2010).

[59]G. Raghurama and R. Narayan, J. Phys. Chem. Solids **44**, 633 (1983).
[60]W. L. Vos, L. W. Finger, R. J. Hemley, and H.-k. Mao, Phys. Rev. Lett. **71**, 3150 (1993).
[61]W. L. Mao, H. kwang Mao, A. F. Goncharov, V. V. Struzhkin, Q. Guo, J. Hu, J. Hu, R. J. Hemley, M. Somayazulu, and Y. Zhao, Science **297**, 2247 (2002).
[62]B. Massani, L. J. Conway, A. Hermann, and J. Loveday, J. Chem. Phys. **151**, 104305 (2019).
[63]V. S. Efimchenko, M. A. Kuzovnikov, V. K. Fedotov, M. K. Sakharov, S. V. Simonov, and M. Tkacz, J. Alloys Compd. **509**, 860 (2011).
[64]M.-E. Donnelly, P. Teeratchanan, C. L. Bull, A. Hermann, and J. S. Loveday, Phys. Chem. Chem. Phys. **20**, 26853 (2018).
[65]Y. Huang, C. Zhu, L. Wang, J. Zhao, and X. C. Zeng, Chem. Phys. Lett. **671**, 186 (2017).
[66]T. Matsui, T. Yagasaki, M. Matsumoto, and H. Tanaka, J. Chem. Phys. **150**, 041102 (2019).
[67]Z. Liu, J. Botana, A. Hermann, S. Valdez, E. Zurek, D. Yan, H. Q. Lin, and M. S. Miao, Nat. Commun. **9**, 951 (2018).
[68]O. Ruff and L. Staub, Z. Anorg. Allg. Chem. **212**, 399 (1933).
[69]R. D. Euler and E. F. Westrum, J. Phys. Chem. **65**, 1291 (1961).
[70]D. Mootz and W. Poll, Z. Naturforsch. B **39**, 290 (1984).
[71]S. I. Troyanov, Crystallogr. Rep. **50**, 773 (2005).
[72]A. J. C. White and C. W. F. T. Pistorius, J. Solid State Chem. **4**, 195 (1972).
[73]G. Natta and R. Rigamonti, Gazz. Chim. Ital. **66**, 762 (1936).
[74]W. T. Foley and P. A. Giguère, Can. J. Chem. **29**, 123 (1951).
[75]I. Olovsson, D. H. Templeton, S. Rundqvist, E. Varde, and G. Westin, Acta Chem. Scand. **14**, 1325 (1960).
[76]R. W. Carlson, Science **283**, 2062 (1999).
[77]M. J. Loeffler and R. A. Baragiola, J. Phys. Chem. A **115**, 5324 (2011).
[78]P. W. Albers, J. Glenneberg, K. Refson, and S. F. Parker, J. Chem. Phys. **140**, 164504 (2014).
[79]K. Sonnenberg, L. Mann, F. A. Redeker, B. Schmidt, and S. Riedel, Angew. Chem., Int. Ed. **59**, 5464 (2020).
[80]V. K. Davis, C. M. Bates, K. Omichi, B. M. Savoie, N. Momčilović, Q. Xu, W. J. Wolf, M. A. Webb, K. J. Billings, N. H. Chou, S. Alayoglu, R. K. McKenney, I. M. Darolles, N. G. Nair, A. Hightower, D. Rosenberg, M. Ahmed, C. J. Brooks, T. F. Miller, R. H. Grubbs, and S. C. Jones, Science **362**, 1144 (2018).
[81]J. Chun, C. Jo, S. Sahgong, M. G. Kim, E. Lim, D. H. Kim, J. Hwang, E. Kang, K. A. Ryu, Y. S. Jung, Y. Kim, and J. Lee, ACS Appl. Mater. Interfaces **8**, 35180 (2016).
[82]B. Dereka, Q. Yu, N. H. Lewis, W. B. Carpenter, J. M. Bowman, and A. Tokmakoff, Science **371**, 160 (2020).
[83]J. H. Clark, J. Emsley, D. J. Jones, and R. E. Overill, J. Chem. Soc. Dalt. Trans. **1981**, 1219.
[84]C. Glidewell, J. Mol. Struct.: THEOCHEM **85**, 365 (1981).
[85]F. Kraus, S. A. Baer, and M. B. Fichtl, Eur. J. Inorg. Chem. **2009**, 441.
[86]S. I. Ivlev, T. Soltner, A. J. Karttunen, M. J. Mühlbauer, A. J. Kornath, and F. Kraus, Z. Anorg. Allg. Chem. **643**, 1436 (2017).